Photoinduced Processes in Riboflavin: Superposition of $\pi\pi^*-n\pi^*$ States by Vibronic Coupling, Transfer of Vibrational Coherence, and Population Dynamics under Solvent Control

Alexander Weigel, Alexander L. Dobryakov, Manoel Veiga,† and J. Luis Pérez Lustres*

Institut für Chemie, Humboldt Universität zu Berlin, Brook Taylor Str. 2, 12489 Berlin, Germany

Received: July 7, 2008; Revised Manuscript Received: September 8, 2008

Femtosecond dynamics of riboflavin, the parent chromophore of biological blue-light receptors, was measured by broadband transient absorption and stationary optical spectroscopy in polar solution. Rich photochemistry is behind the small spectral changes observed: (i) loss of oscillator strength around time zero, (ii) sub-picosecond (ps) spectral relaxation of stimulated emission (SE), and (iii) coherent vibrational motion along a' (in-) and a'' (out-of-plane) modes. Loss of oscillator strength is deduced from the differences in the time-zero spectra obtained in water and DMSO, with stationary spectroscopy and fluorescence decay measurements providing additional support. The spectral difference develops faster than the time resolution (20 fs) and is explained by formation of a superposition state between the optically active ($^1\pi\pi^*$) S_1 and closely lying dark ($^1n\pi^*$) states via vibronic coupling. Subsequent spectral relaxation involves decay of weak SE in the blue, 490 nm, together with rise and red shift of SE at 550 nm. The process is controlled by solvation (characteristic times 0.6 and 0.8 ps in water and DMSO, respectively). Coherent oscillations for a' and a'' modes show up in different regions of the SE band. a'' modes emerge in the blue edge of the SE and dephase faster than solvation. In turn, a' oscillations are found in the SE maximum and dephase on the solvation timescale. The spectral distribution of coherent oscillations according to mode symmetry is used to assign the blue edge of the SE band to a $^1n\pi^*$-like state (A″), whereas the optically active $^1\pi\pi^*$ (A′) state emits around the SE maximum. The following model comes out: optical excitation occurs to the Franck−Condon $\pi\pi^*$ state, a $\pi\pi^*-n\pi^*$ superposition state is formed on an ultrafast timescale, vibrational coherence is transferred from a' to a'' modes by $\pi\pi^*-n\pi^*$ vibronic coupling, and subsequent solvation dynamics alters the $\pi\pi^*/n\pi^*$ population ratio.

Introduction

Flavins (Scheme 1) are redox-active chromophores of respiratory enzymes, and they represent a newly discovered class of blue-light receptors.[1,2] Photoreceptors are proteins binding a chromophore cofactor. Absorption of light by the chromophore induces a primary structural change on it, which is known as activation step. By means of protein−chromophore frictional forces and/or chemical reactions, the primary structural change propagates from the protein pocket to the surface to render the so-called light-adapted state. The final conformation is metastable, which can eventually revert to the dark-adapted state, is not formed thermally and is responsible for a light-induced biological response. It follows that function and structure are intimately linked through all relevant time scales. Therefore, the function−structure tandem is susceptible of being studied by ultrafast spectroscopic techniques.

There are six families of photoreceptors: rhodopsins, phytochromes, xanthopsins, cryptochromes, phototropins, and BLUF-domain containing proteins.[2] The first three families make use of phytochromobilin, retinals, and coumaric acid, respectively, as chromophore cofactors, and it is well established that the primary activation step involves E/Z isomerization of the chormophore.[2] The last three families bind flavin derivatives.

SCHEME 1: Molecular Structures of Riboflavin and Lumiflavin

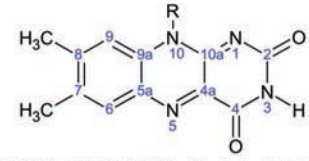

R=$CH_2(CHOH)_3CH_2OH$ (Riboflavin), CH_3 (Lumiflavin)

They show a great variety of functions such as control of the circadian clock in mammals, insects, and plants (cryptochromes), chloroplast movement or phototropism (LOV domains in phototropins), and photosynthesis gene expression and photophobic responses (BLUF proteins). In this case, the rigid structure of flavin precludes activation by E/Z isomerization.

The striking ability of flavin to display distinct and various protein-specific activation mechanisms motivated this work.[3] For instance, signaling state formation in BLUF domains occurs on a time scale of ∼100 ps in the singlet manifold[4] and seems to mainly alter the short range interactions in the protein pocket.[5−7] Electron- and proton-transfer processes have recently been suggested by Gauden et al., who also proposed a 180° rotation of a highly conserved glutamine residue as key process for stabilizing the signaling state.[8] On the contrary, for LOV domains, it is well established that the signaling state forms on the microsecond timescale via the triplet state and involves a covalent cysteine−flavin adduct.[9−12] Much less is known about

* Corresponding author. E-mail: lustres@chemie.hu-berlin.de. Phone: +49 (0)30 2093 5546. Fax: +49 (0)30 2093 5553.

† during leave from Departamento de Química Física, Universidad de Santiago de Compostela, Avda. das Ciencias s/n, 15782 Santiago de Compostela (Spain).

10.1021/jp805962u CCC: $40.75 © 2008 American Chemical Society
Published on Web 11/04/2008

early stages in the cryptochrome photocycle; only recently, Kottke et al.[13] found evidence of FAD neutral radical formation with small changes in the secondary structure of the protein *At*cry1.[3]

Riboflavin was chosen as model compound among the biologically relevant flavin-based chromophors. Riboflavin may exist in various redox structures in the ground state: the oxidized flavoquinone, the semireduced flavosemiquinone, and the fully reduced flavohydroquinone, each of which yields various acid base forms depending on pH.[14] We focus on the neutral oxidized form, the one bound by blue-light receptors. The neutral oxidized form (RF) can be prepared in the ground state and selectively excited. It shows pK_a values of 0.4 for protonation at N_1 and 9.8 for deprotonation at N_3-H, and therefore, it is dominant in the pH range from 2 to 8 and in polar solvents.[15]

The $S_1 \leftarrow S_0$ vertical transition has nearly no charge-transfer character as deduced from solvatochromism[16−18] and Stark effect spectroscopy (or electroabsorption).[19] Quantum mechanical calculations in RF and derivatives at different levels of theory[20−24] show important variance and thereby fail to reproduce this important result. Values from refs 20 and 24 appear to be consistent with experiment, that is, with the lack of charge-transfer character for the vertical $S_1 \leftarrow S_0$ transition. RF fluoresces from the $\pi\pi^*$ S_1 state with ∼20% quantum yield and ∼5 ns lifetime in neutral water.[15,16,25] Efficient S_1 fluorescence quenching by electron donors,[26−28] aromatic aminoacids,[29−33] and purines[26,34,35] has been explained by electron transfer to the excited flavin in the S_1 state. The process reverts quantitatively to the oxidized neutral form, and radical species do not build up. In contrast, the triplet state (which is formed with ∼20−30% quantum yield in aqueous solution)[36] is well-known to be the reactive species in flavin photo-reduction, -dealkylation, and -addition reactions.[37]

Quasi-forbidden $^1n\pi^*$ states (allowed by symmetry but dark because of small orbital overlap) were allocated close to the S_1 and S_2 states by quantum mechanical calculations.[20,22,23,38,39] Experimental indication for $\pi\pi^*-n\pi^*$ vibronic coupling was found by fluorescence/phosphorescence polarization spectroscopy, most clearly for alloxazines.[39] The coupling is thought to explain redox activity of flavins in the triplet manifold,[37] enhanced intersystem-crossing rate,[23] solvent and temperature dependence of the non-radiative rate constant for S_1 deactivation, and the effect of electron-donating groups on the luminescence properties of riboflavin.[39]

Despite the rich behavior outlined in the preceding paragraphs, only few picosecond studies have been carried out with bare flavin-based chromophores,[34,35,40,41] most of which deal with the mechanism of fluorescence quenching.[34,35,41] A number of papers were devoted to the femtosecond dynamics of complex systems such as flavin-based enzymes[31−33,42] and photoreceptors.[4,8,43−47] In contrast, the information available about the early evolution of the flavin chromophore in solution is limited. In the only paper so far,[40] Petushkov et al. examined the picosecond-resolved fluorescence of riboflavin and lumiflavin in aqueous solution with 400 nm excitation and assigned the spectral evolution to solvation dynamics.

In the present paper, we attempt to extend current knowledge on excited-state flavin dynamics. A comprehensive account of the stationary optical spectroscopy and femtosecond broadband transient absorption of RF in water and DMSO is provided. Stationary spectroscopy is used in combination with time-resolved fluorescence to measure transition dipole moments for the $S_1 \leftrightarrow S_0$ transition and to estimate the solvation contribution to the Stokes shift. In the femtosecond experiment,[48] we enlarge the spectral window towards the UV and near-IR and trace the spectral evolution back to the first femtoseconds after photon absorption. Simultaneous measurement of the full transient spectrum in a single laser shot enables high photometric accuracy, because spectral reconstruction is not necessary.

We capture an ultrafast loss of oscillator strength at earliest time. Further evidence is obtained by stationary spectroscopy of the $S_1 \leftrightarrow S_0$ transition. $^1n\pi^*-^1\pi\pi^*$ vibronic coupling accounts for this finding. Structural relaxation along low-frequency modes and solvent-controlled $^1n\pi^* \rightarrow ^1\pi\pi^*$ conversion are proposed to be behind the small spectral evolution on the sub-picosecond timescale. Coherent vibrational motion along in-plane (a') and out-of-plane (a'') low-frequency modes is observed. Symmetric and non-symmetric oscillations localize in adjacent regions of early stimulated emission. The latter demonstrates non-adibatic mixing of $^1n\pi^*$ (A″)- and $^1\pi\pi^*$ (A′)-like states on a ultrafast timescale (20 fs). Thus, vibrational coherence is transferred from the Franck−Condon $^1\pi\pi^*$ state to the $^1n\pi^*$ state.[49] Subsequent $^1n\pi^*-^1\pi\pi^*$ conversion is controlled by solvent motion.

Experimental Section

(−)-Riboflavin was purchased from Sigma-Aldrich (≥98%) and used without further purification. Solutions were freshly prepared in spectroscopic grade solvents (Aldrich) and deionized water. Buffer solutions (pH = 7.00, 8.00 at 20 °C, CertiPUR, Merck) yielded the same results as deionized water. pH was controlled with a CG-842 SCHOTT pH-meter equipped with a combined glass electrode.

UV−vis absorption spectra were scanned on a Varian Cary 300. Fluorescence spectra were obtained on a Spex Fluorolog-2 spectrofluorimeter, corrected for instrumental factors and transformed into cross-section for stimulated emission, the counterpart of absorption cross-section.[50] Fluorescence quantum yields were measured relative to aqueous quinine sulfate[51] and rhodamine 101 in ethanol[52] as fluorescence standards. Fluorescence lifetimes were determined by single-photon counting on an Edinburgh Analytical Instruments (EAI) CD900 spectrofluorimeter equipped with a hydrogen-filled gas lamp (350 nm excitation, 40 kHz rep. rate, 0.2 ns resolution) and with a Lifespec (EAI) with excitation at 333 and 370 nm (2.5 MHz rep. rate, 10−50 ps resolution).

The femtosecond pump-supercontinuum probe (PSCP) setup has been described elsewhere.[48,53] Briefly, $\sim 10^{-4}$ mol dm^{-3} sample solutions were flowed through a thin quartz cell (0.4 mm). Two femtosecond laser sources were used: a Ti:Sa oscillator-regenerative amplifier laser system (CPA 2001, Clark MXR), which drives two non-collinear optical parametric amplifiers (NOPA) at 150 Hz repetition rate, and a Ti:Sa oscillator-multipass amplifier system (Femtolasers, 150 Hz), which drives a collinear optical parametric amplifier (TOPAS, Light Conversion). For the first setup, a single stage NOPA was used to excite the sample with 490 nm, 0.5 μJ, ∼30 fs pulses focused to a spot size of 100 μm. A white light continuum was generated by focusing the output of the second NOPA (6 μJ, 25 fs pulses at 530 nm) onto a 1 mm thick CaF_2 plate. In the second case, the TOPAS was tuned to 440 nm (0.5 μJ, 40 fs pulses, 100 μm spot size) and used as excitation source. Second harmonic of the Ti:Sa fundamental was also used as excitation source and for continuum generation with similar parameters as above. The white-light continuum was spectrally filtered, split for reference, and 1:1 imaged onto the sample cell. Reference and transmitted beams were imaged onto the entrance slits of separate home-build grating spectrographs. Transient spectra were registered with photodiode arrays (Hamamatsu, S3901Q,

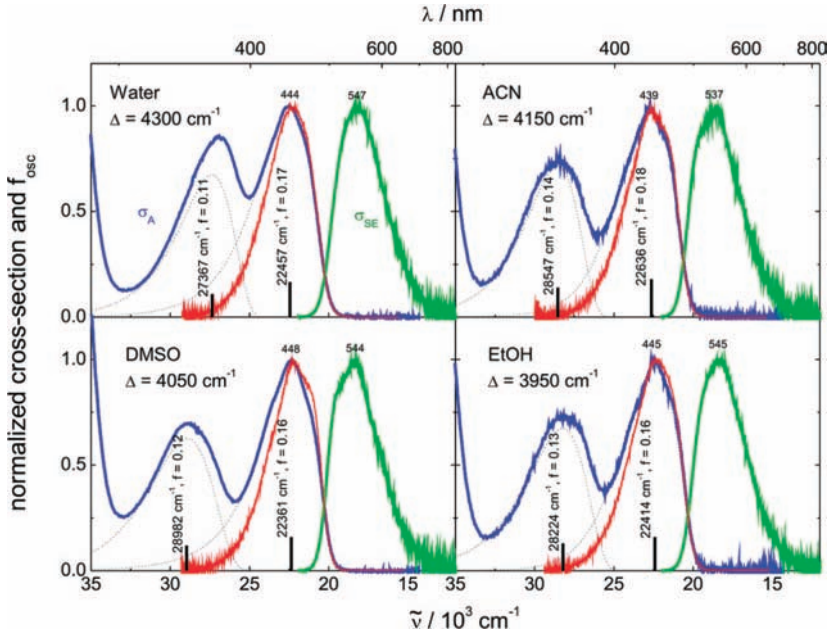

Figure 1. Peak-normalized cross-sections for absorption (σ_A, blue solid line) and stimulated emission (σ_{SE}, green solid line) of riboflavin in water, acetonitrile (ACN), dimethylsulfoxide (DMSO), and ethanol (EtOH). Positions of maxima in nanometers are indicated on top of the fluorescence and first absorption bands. The low-energy part of the absorption spectra was decomposed into two optically allowed transitions (black dotted lines) by a log-normal fit. Absorption maxima (cm^{-1}) and oscillator strengths f_{0i} for each $S_i \leftarrow S_0$ transition are indicated by vertical bars. σ_{SE} was also reflected around its maximum and blue-shifted by Δ (red solid lines).

TABLE 1: Photophysical Properties of the $S_1 \leftrightarrow S_0$ Electronic Transition of RF[a]

solvent	Φ_F	τ/ns [b]	$k_{rad}/10^7$ s^{-1} [c,d]		f_{osc} S_1-S_0 [e]	$\mu_{0\rightarrow1}/D$	$\mu_{1\rightarrow0}/D$ [f]	$2\Lambda/cm^{-1}$	
			SB	Φ_F/τ				shifts[g]	maxima[g]
water	0.2	4.7	6	4	0.17	4.1	3.4−3.7	4300	4360
methanol	0.2	5.4	7	4	0.17	4.1	3.1−3.4	4000	4070
acetonitrile	0.3	5.9	8	5	0.18	4.3	3.5−3.8	4150	4090
DMSO	0.1	2.9	8	4	0.16	4.1	2.6−2.9	4050	4110
ethanol	0.2	5.4	7	4	0.16	4.1	3.0−3.3	3950	4070

[a] Fluorescence quantum yield (Φ_F), fluorescence lifetime (τ), radiative rate constant for absorption and emission (k_{rad}), oscillator strength (f_{osc}), transition dipole moments ($\mu_{i\rightarrow j}$), and Stokes shift (2Λ) of riboflavin in polar solution. [b] The fluorescence decay of riboflavin is slightly non-exponential. Only the major component is considered, see text. [c] The radiative rate constant was calculated with the Strickler−Berg[56] formula for absorption (column head SB). The radiative constant for emission was obtained from the ratio Φ_F/τ as indicated in the corresponding column head. [d] The Strickler−Berg formula has a precision better than 10% for $\varepsilon_{max} \geq 10 \times 10^3$ mol^{-1} dm^3 cm^{-1} and well-separated absorption bands. The observed differences between the SB and fluorescence values is therefore beyond experimental precision. [e] Oscillator strengths from quantum mechanical calculations are ~0.2,[20] 0.14,[22] and 0.24.[23] [f] Transition dipole moments for emission were calculated according to Lewis, J. E.; Maroncelli, M. *Chem. Phys. Lett.* **1998**, *282*, 197. [g] Stokes shift was measured from the differences between the spectral maxima for absorption and fluorescence and by blue-shift of the mirror imaged stimulated emission cross section, see Figure 1.

512 pixels) at ~2 nm spectral resolution. Baseline-corrected transient absorption spectra were calculated for single shots, and typically, 50 shots were averaged. Final signal is typically obtained by averaging five independent scans, so that the photometric noise becomes $\sim 10^{-4}$ OD. Pump−probe cross-correlation over the full spectral window ranges from 50 fs (FWHM around 400 nm) to 70 fs (in the UV), and the time resolution is estimated to be 20 fs on average. Solvent contribution was not subtracted. No photodegradation was observed on a day to day basis.

Results

Absorption Transition Dipole, Stokes Shift, and Lineshapes from Stationary Spectroscopy. Steady-state spectroscopy was used to measure transition dipole moments for the $S_1 \leftrightarrow S_0$ transition,[50] to estimate the solvation contribution to the Stokes shift, and to compare the absorption and emission lineshapes.

UV−vis absorption and stimulated emission cross-sections of RF in polar solution are shown in Figure 1. The absorption spectrum was fitted to a sum of log-normal functions[54,55] to separate the first three optically allowed transitions. The $S_1 \leftarrow S_0$ transition has an oscillator strength f_{01} of 0.17 in water, consistent with quantum mechanical calculations, Table 1.[20,22,23] For the $S_1 \leftarrow S_0$ transition, absorption properties are independent of solvent. On average, we obtain an oscillator strength f_{01} of 0.17; a transition dipole moment μ_{01} of 4.1 Debye and a radiative rate constant k_{01} of 7×10^7 s^{-1} as calculated by the Strickler−Berg formula, Table 1.[50,56] Oscillator strengths of 0.11 and 0.48 were obtained for the $S_2 \leftarrow S_0$ and the $S_3 \leftarrow S_0$ transitions, respectively.

The measured fluorescence quantum distribution $F(\lambda)$ was transformed into cross-sections for stimulated emission $\sigma_{SE}(\lambda)$. A moderate Stokes shift Δ of about 4000 cm^{-1} is obtained from the difference between absorption and stimulated emission maxima, eq 1 and Table 1. A guess of the intramolecular

contribution λ_{intra} can be obtained from the Stokes shift in non-polar alkanes,[57] but because RF does not dissolve in non-polar solvents, one can at least set an upper limit with the Stokes shift in the protein environment of the LOV−his domain, $2\lambda_{intra} \leq 3400\ cm^{-1}$.[58] It turns out that the solvent reorganization energy is given by $2\lambda_{solv} = 2\Lambda - 2\lambda_{intra} \geq 500\ cm^{-1}$, eq 1. The estimate is in line with the dynamic Stokes shift resolved by transient fluorescence: 240 cm^{-1}.[40]

$$\Delta = 2\Lambda = 2\lambda_{intra} + 2\lambda_{solv} \quad (1)$$

Cross-sections for stimulated emission were mirror imaged at their maxima and blue-shifted by Δ to match the first absorption band, as shown in Figure 1. The values of Δ are quoted in Figure 1 and Table 1 for polar solvents. They are consistent to within 100 cm^{-1} with the Stokes shifts obtained from the difference between absorption and stimulated emission maxima. Absorption and stimulated emission show comparable spectral shapes. DMSO is the only case where the main Franck−Condon progression shows noticeable differences between absorption and emission. The latter effect points towards coupling of the main optically-active high-frequency mode to low-frequency modes. We also note that stimulated emission is clearly narrower than the first absorption band in all solvents. The estimated absorption broadening is $\delta\varepsilon \approx 500\ cm^{-1}$. By applying the uncertainty principle $\delta\varepsilon \approx \hbar/\tau$, a 500 cm^{-1} broadening leads to a lifetime of about 10 fs for the Franck−Condon state.

Fluorescence Transition Dipoles. Fluorescence quantum yields (Φ_F) and lifetimes (τ) were measured in all solvents where RF solubility enables accurate measurements, Table 1. The radiative rate constant for fluorescence was obtained ($k_{rad} = \Phi_F/\tau$) and used to calculate the $S_1 \rightarrow S_0$ transition dipole,[50,59] with the implicit assumption that no static quenching occurs. It was found that the fluorescence radiative rate constant k_{10} and transition dipole μ_{10} are significantly lower than those for absorption, Table 1. The rate of radiationless processes seems to depend on specific solute-solvent interactions because RF has the highest fluorescence quantum yield in acetonitrile and the lowest in DMSO, whereas the fluorescence decay rates show the opposite trend.

To summarize, important differences are observed in the transition dipole moments for $S_1 \leftrightarrow S_0$ absorption and emission, the latter being 15−30% smaller. The Stokes shift amounts to ~4000 cm^{-1}, from which at least 500 cm^{-1} correspond to solvent reorganization. Absorption and fluorescence lineshapes are comparable, although in DMSO, the main Franck−Condon progression is noticeably different for absorption and emission. Absorption lineshapes are about 500 cm^{-1} broader than fluorescence, pointing to an ultrafast (~10 fs) process in the Franck−Condon state.

Femtosecond Transient Absorption Spectroscopy in Water. Femtosecond broadband transient absorption of RF in water (pH = 7) and DMSO was measured with excitation at 400, 440, and 490 nm. For direct assessment, only the raw spectral evolution from excitation at 440 nm in water and DMSO will be shown here. The spectral evolution for excitation at 400 and 490 nm is summarized in the Supporting Information.[60]

Transient spectra recorded in water (pH = 7) with ~2000 cm^{-1} excess excitation energy (λ_{exc} = 440 nm) are shown in Figure 2. They display the signatures of negative $S_1 \leftarrow S_0$ absorption (bleach), $S_n \leftarrow S_1$ excited-state absorption (ESA), and $S_1 \rightarrow S_0$ fluorescence in the form of stimulated emission (SE). Spectral change is modest at first sight but nonetheless distinguishable. Earliest evolution becomes visible under these conditions, that is, when excitation at the spectral maximum in a solvent of low refractive index and distant resonances results in a small non-resonant coherent contribution from the solvent.[48] Rich vibrational structure is observed in SE and bleach at early time, panel a. Vibronic progressions along modes with frequencies of ~300 and ~1200 cm^{-1} are apparent in the bleach band.[60] Early vibronic structure of SE is more involved because of ultrafast relaxation of hot fluorescence on a 50 fs time scale. Vibrational structure washes out very fast (characteristic time constant $\tau < 20$ fs) and in effect follows the cross-correlation. During the first two picoseconds, panel b, ESA rises at 500 nm, and the SE band shifts to the red by 400 cm^{-1}. The shift is also noticeable on the red edge of the SE band. On the 500 ps timescale, small spectral changes follow, panels c and d. Bleach amplitude decreases, whereas SE increases marginally, and the ESA band around 300 nm clearly decays. Afterwards, the full transient spectrum decays with nearly constant shape on the nanosecond time scale. The non-decaying component on the 2 ns scale is assigned to the triplet state (see Supporting Information).[60]

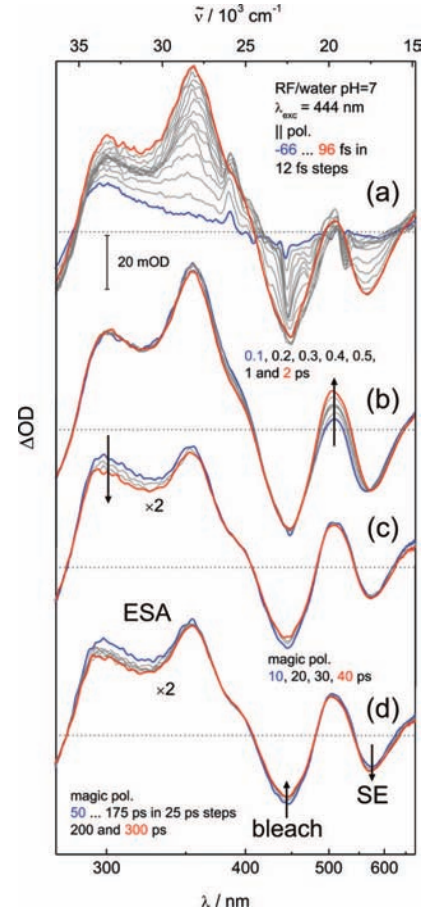

Figure 2. Transient absorption spectra of riboflavin in water (pH = 7) after excitation at 440 nm. (a) Spectral evolution as pump and probe pulses overlap in time. (b) Spectral evolution up to 2 ps at parallel polarization. (c) evolution up to 40 ps at magic-angle polarization. (d) evolution up to 300 ps at magic-angle polarization. Spectra were multiplied by 2 in panels c and d. Horizontal dotted lines indicate the zero-signal level for each panel. Blue and red spectra are the first and last spectra for every series, respectively. Pump−probe delays are given as insets, and signal amplitudes are given by the inner gauge. Note that in panel b, the spectral evolution at wavelengths below 350 nm is distorted because of longer cross-correlation in the UV.

Figure 3 highlights the spectral differences induced when femtosecond excitation pulses are tuned across the first electronic transition of riboflavin. Transient spectra obtained for 400 and

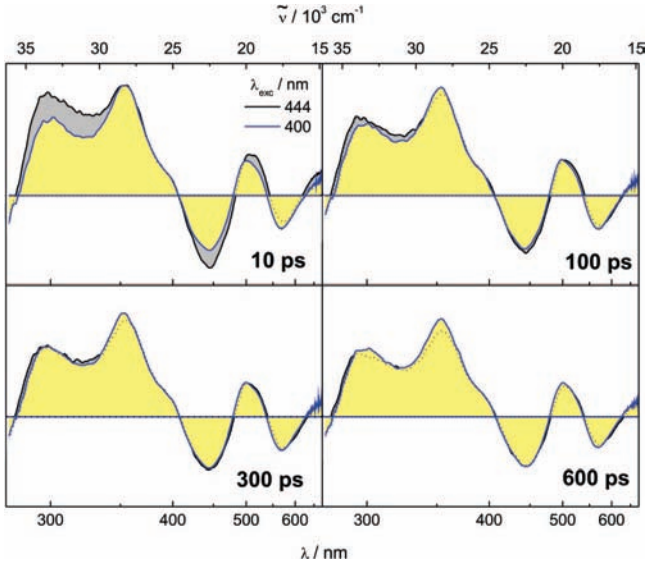

Figure 3. Transient absorption spectra of riboflavin in water (pH = 7) are compared for excitation wavelengths 400 (blue, yellow filled) and 440 nm (black, gray filled). Horizontal dotted lines denote the zero signal level. Each frame corresponds to a single pump−probe delay as indicated. Measurements were normalized in the peak of the bleach band at 2 ns delay. All spectra were obtained with magic-angle polarization.

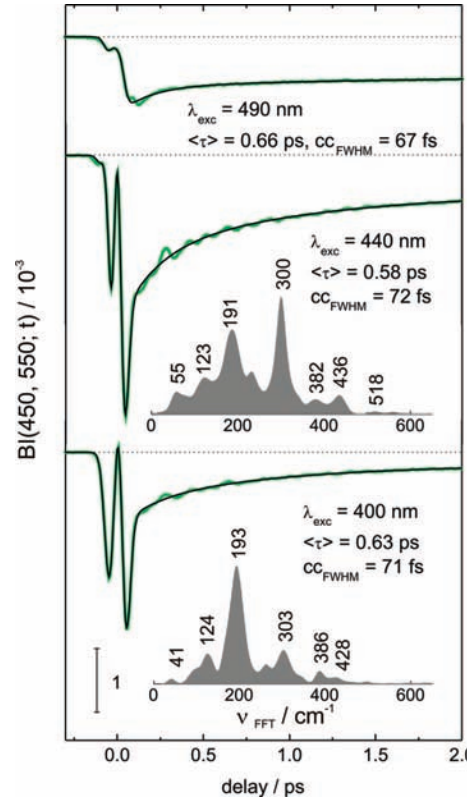

Figure 4. Band integrals between 450 and 550 nm (thick green line) for riboflavin in water and their biexponential fits (black solid line) for excitation at 490 (top), 440 (middle), and 400 nm (bottom). The ordinate scale is defined by the inner gauge, and dotted horizontal lines mark the zero band-integral level of each frame. The inset gives the cross-correlation width (cc_{FWHM}, assuming a Gaussian pulse shape) and the characteristic time constant $\langle\tau\rangle$ calculated as weighted average of the two time constants in the biexponetial fit, see text. Fourier power spectra of residuals are shown for the excitations at 440 and 400 nm, where an oscillatory contribution to the band integral is observed (gray-filled spectra).

440 nm pumping are compared at the pump−probe delays 10, 100, 300, and 600 ps. Substantial increase of ESA is observed for 440 nm excitation at 10 ps delay, most clear in the red flank of the SE band and in the ESA bands centred at 500 and 300 nm. The difference vanishes at longer times and, already at 600 ps, approaches our photometric limit. It is important to realize that this behaviour does not reflect vibrational cooling of the flavin for two reasons. First, in case of vibrational cooling, the early spectral broadening increases with excess energy, but we observe that 400 and 490 nm excitations yield similar spectra, whereas larger differences are found upon 440 nm excitation. Second, different excitations converge slowly to the same spectrum but on the 500 ps time scale. This is too long for vibrational thermalization of a molecule this size, where a timescale of ∼10 ps is expected for vibrational cooling.[61]

A band integral analysis was performed in order to characterize early spectral dynamics. Band integrals

$$\mathrm{BI}(\lambda_1, \lambda_2; t) \equiv \int_{\lambda_1}^{\lambda_2} \frac{\Delta\mathrm{OD}(\lambda, t)}{\lambda}\, \mathrm{d}\lambda$$

are proportional to the transition dipole moment squared[50] and are preferred over kinetic traces at single wavelengths because they minimize distortion of the pure population/oscillator strength dynamics by spectral diffusion, broadening, or narrowing. BIs calculated between 450 and 550 nm display biexponential behavior. A characteristic time constant τ is defined as a weighted average of both exponential time constants τ_1 and τ_2. Thus, $\langle\tau\rangle \equiv (a_1\tau_1 + a_2\tau_2)/(a_1 + a_2)$, where a_1 and a_2 are the associated amplitudes. We find that $\langle\tau\rangle \approx 0.6$ ps in water does not depend on excitation wavelength within experimental precision, Figure 4. Precision is limited here by the very small amplitude of spectral changes rather than by the pump−probe cross-correlation width. The characteristic time constant matches within error the water solvation time of 0.5 ps.[62] Weak oscillations appear and rapidly dephase during the first picosecond, but they were not included in the model function at this stage. The Fourier power spectra of residuals show strong peaks at 300 and 190 cm^{-1} plus minor features at lower and higher frequencies. Note however that these oscillations are seen only at excitations with excess of energy. The band integral for 490 nm pumping is essentially free of oscillatory components in water.

A global analysis of band integrals for magic-angle polarization was performed on the timescale extending to 600 ps.[60] Nanosecond components were constrained in the fitting procedure to a narrow interval around the fluorescence lifetime. The latter were measured with higher accuracy by single-photon counting (Table 1). The signal decays multi-exponentially, especially upon 440 nm excitation where two decay times are identified: ∼100 ps and 4.6 ns. These values are difficult to determine because of (i) the small contribution of the ∼100 ps component and (ii) the big difference between the scanned time window of 600 ps and the fluorescence lifetime of 4.6 ns. Hence, only qualitative understanding may be gained. The slowest component is assigned to the (relaxed) $S_1 \rightarrow S_0$ decay. The other component, ∼100 ps, is visible over the full spectral window.[60] It characterises the signal decay in the ESA at 300 nm and bleach regions, suggesting that population is leaving the excited state and returns to S_0. This finding contrasts with fluorescence up-conversion data where a 36 ps time constant was observed with negative amplitude, indicating a rise in the cross-section for SE on the 100 ps timescale.[40] Therefore, spectral dynamics with 40−100 ps time constant may reflect time-evolution of oscillator strength rather than S_1-S_0 conversion.

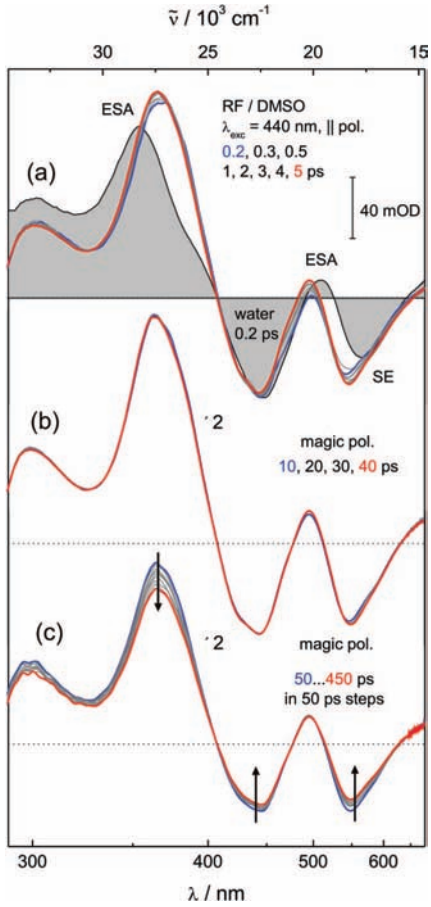

Figure 5. Transient absorption spectra of riboflavin in DMSO at the indicated pump−probe delays for 440 nm excitation. (a) Transient spectra during the earliest 5 ps at parallel pump−probe polarization. The gray-filled spectrum was obtained in water at 0.2 ps delay in otherwise equal experimental conditions. (b) Spectral evolution up to 40 ps at magic-angle polarization. (c) Spectral evolution between 50 and 450 ps at magic-angle polarization. Further details are the same as in Figure 2.

Band integrals for 490 and 400 nm excitation contain 60−70 ps decays with even smaller amplitude. However their order of magnitude and spectral distribution hint at the same underlying process, which is triggered at 440 nm with higher efficiency. Thus, the ∼100 ps time constant is associated with the transient spectral differences outlined in Figure 3. The difference vanishes after 500 ps.

Femtosecond Transient Absorption Spectroscopy in DMSO. Transient absorption of RF in DMSO upon 440 nm excitation is shown in Figure 5. Water and DMSO are quite similar solvents in terms of non-specific polarity. They have different dielectric constants ε (80.10 and 47.24 at 20 °C) and refractive indexes n (1.3334 and 1.4170 at 20 °C), but what matters for dipolar solvation is the function $\Delta f(\varepsilon, n) = (\varepsilon - 1)/(2\varepsilon + 1) - (n^2 - 1)/(2n^2 + 1)$. The latter is practically equal for both: 0.32 for water and 0.28 for DMSO. In regard of specific solute−solvent interactions concerns, DMSO has no interchangeable protons so that prototropic and/or acid−base equilibria of RF can be ruled out. It also interacts more weakly by hydrogen bonding, having only proton-acceptor character, whereas water behaves both as donor and acceptor. Altogether, DMSO switches off several degrees of freedom compared to water while keeping the same polarity. Transient spectra in DMSO evolve however similarly as in water. This observation suggests that the behaviour described for water solution is not directly related to specific solute−solvent interactions or solute−solvent proton-transfer processes. During the earliest 5 ps, rise of ESA around 500 nm is observed, whereas only minor changes occur in other spectral regions, Figure 5 top. A 200 cm^{-1} red shift of the SE band can be recognized in the blue and red flanks. The spectral shape stays practically constant later on and decays on nanosecond time scale, Figure 5 bottom. A long-living component remains and is assigned to the triplet state (not shown). Remarkably, the spectrum measured at early time differs substantially from that observed in neutral aqueous solution at the same excitation wavelength. The same bleach, ESA and SE bands are found, but they show up with different amplitudes. This effect is especially clear upon 490 nm excitation, where the amplitude of the SE in water amounts only to half the amplitude in DMSO.[60]

Spectral dynamics of RF in DMSO was also characterized by band integral analysis, Figure 6. During the earliest 2 ps, Figure 5a, the only remarkable change is the rise of an ESA band around 500 nm. The band integral between 450 and 550 nm was formed and fitted to a biexponential function while modelling the coherent contribution around time zero.[48] Oscillatory terms were not included in the model function, and main oscillation frequencies are estimated from a Fourier analysis of residuals. The top panel in Figure 6 shows the corresponding signal of the pure solvent due to its nonresonant coherent contribution. The residuals contain damped oscillations induced by impulsively stimulated Raman scattering of the solvent at early time. Frequencies of 313, 351, 401, and 676 cm^{-1} are obtained by Fourier analysis, and they match the Raman spectrum of DMSO. For excitation of RF at 400 and 490 nm, the characteristic time constants obtained in this way are the same, 0.9 ps. Pronounced RF oscillations occur at ∼190 and 300 cm^{-1} together with broad features at lower frequencies, Figure 6, especially upon 400 nm excitation where two damped oscillations with ∼50 and ∼100 cm^{-1} frequencies are clearly visible.

In the 600 ps time window, the band integrals deviate only slightly from exponential behaviour.[60] Band integrals were analyzed globally for every excitation wavelength. As in the case of water, nanosecond time constants were forced to match the fluorescence decay time, whereas other components were set free in the fitting procedure. A 100−400 ps time constant was found over the full spectral window but with very small amplitude. The amplitude distribution resembles that found in water for the ∼100 ps time constant, which suggests that both time constants arise from the same process.

Let us sum up the main results obtained from femtosecond transient absorption. An ultrafast loss of oscillator strength is identified by comparing transient spectra in water and DMSO at early time, Figure 5 top. It occurs faster than time resolution, 20 fs. Evolution on the picosecond timescale is mainly seen as increase of ESA at 500 nm, Figures 2b and 5 top. The process was characterised by band integral analysis and shows time constants of 0.6 and 0.9 ps in water and DMSO, respectively, Figures 4 and 6. Oscillatory behaviour was observed. Redistribution of oscillator strength seems to take place with ∼100 ps time constants in water and DMSO.

Discussion

Method of Analysis. Transient absorption spectra were analyzed globally for all excitation wavelengths in water and DMSO with the aim of defining the processes underlying spectral dynamics. The results obtained for water at 440 nm will be shown in this section, and other measurements are

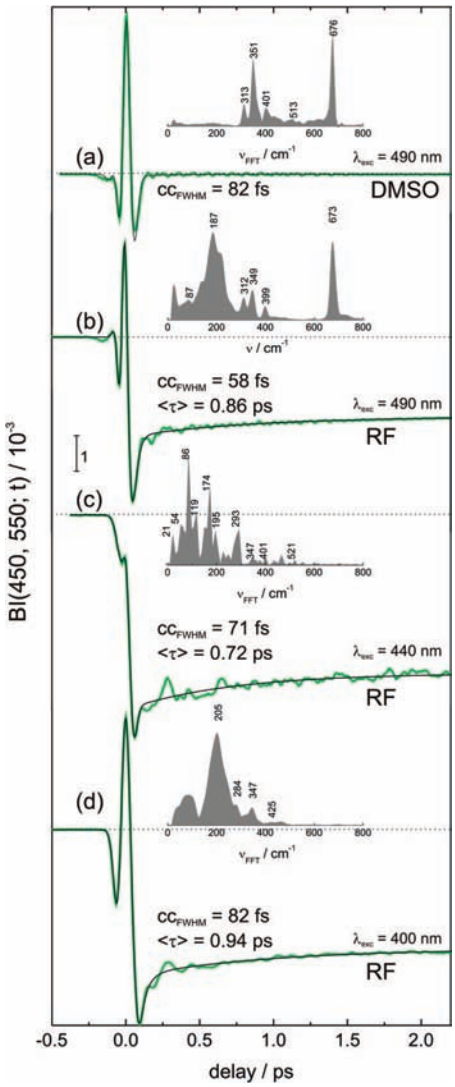

Figure 6. Analysis of band integrals (thick green lines) between 450 and 550 nm for riboflavin in DMSO. (a) Pure DMSO with non-resonant excitation at 490 nm. (b−d) Riboflavin in DMSO with excitation at 490, 400, and 400 nm, respectively. Band integrals were fitted to biexponential model functions plus terms describing the coherent contribution (thin black line). Characteristic time constants for the processes are given as insets together with the cross-correlation (cc_{FWHM}) and the Fourier power spectra of residuals (gray-filled spectra). Main Fourier peaks are labelled. The ordinate scale is defined by the inner gauge and dotted horizontal lines mark the zero band-integral level of each frame.

summarized in Table 2 and described in the Supporting Information.[60]

The sequential contribution $S(\lambda, t)$ to transient absorption spectra[48] was fitted to a sum of n_{exp} exponentials, a sum of n_{osc} cosine-like damped oscillations, and a non-decaying or offset component, eq 2. The coherent contribution $C(\lambda, t)$ to transient absorption was modeled as a sum of a Gaussian function plus its time-derivatives as described in ref 48. Terms were convoluted with the pump−probe cross-correlation $G(t)$ which is assumed to be Gauss-shaped and taken to be constant over the full spectral window. For this reason, the analysis was never extended beyond 350 nm towards the UV because of substantial cross-correlation broadening there. The spectral amplitudes $A(\lambda)$ are obtained by solving the system of n_{delay} linear equations for each probe wavelength λ, where n_{delay} is the number of pump−probe delays scanned on a single measurement.[63] Frequencies, damping constants, decay times, zero delay, and pump−probe cross-correlation were optimized to minimize the difference between the experiment $\Delta OD(t, \lambda)$ and the model function $Y(t, \lambda) = C(t, \lambda) + S(t, \lambda)$. Results from the global fit are shown in Figure 7, where the time evolution in water after 440 nm excitation is described with two exponential functions and three damped oscillations.[64] The average pump−probe cross-correlation over the full window is 65 fs (FWHM), and the modeled coherent contribution (magenta in Figure 7) matches the time evolution of the non-resonant solvent signal (cyan). This may be taken as good indication for adequate separation between resolved and unresolved processes. The latter enter into the coherent contribution, that is, follow the pump−probe cross-correlation.

$$S(t,\lambda) = G(t) \otimes \left[\left\{ \sum_{i=1}^{n_{exp}} A_i(\lambda) \exp[-t/\tau_i] + A_{Offset}(\lambda) + \sum_{j=1}^{n_{osc}} A_j(\lambda) \exp[-t/\tau_j] \cos[\omega_j t + \phi_j(\lambda)] \right\} \Theta(t) \right] \quad (2)$$

Dynamics on the 600 ps timescale is examined by global analysis of band integrals.[60]

We will discuss three main observations which are briefly outlined as follows. First, ultrafast changes in the oscillator strength of SE and ESA are identified at earliest time. They reflect vibronic coupling between the bright $\pi\pi^*$ and dark $n\pi^*$ states, with a coupling strength which may depend on short-range interactions with the nearest environment. Second, exponential dynamics occurs in the sub-picosecond timescale. It monitors $^1n\pi^*-^1\pi\pi^*$ conversion and dynamic shift of the fluorescence band. Both effects are not observed directly because of spectral overlap with ESA, but they can be assessed in combination with fluorescence up-conversion data from the literature, from the analysis of stationary spectra, and global fit of femtosecond transient absorption. Electronic conversion and Stokes shift follow solvation dynamics. Third, weak coherent oscillations are observed in the bleach and SE regions. Analysis of the oscillatory contribution indicates that intramolecular relaxation occurs along in- and out-of-plane nuclear coordinates. Unambiguous optical activity along out-of-plane modes and spectral discrimination between symmetric (A′) and non-symmetric (A″) modes demonstrates vibronic coupling between $^1\pi\pi^*$ (A′) and $^1n\pi^*$ (A″) states. Finally, tiny spectral changes on the 600 ps timescale seem to monitor redistribution of oscillator strength rather than population dynamics. Fluorescence up-conversion experiments favor this interpretation.[40] These observations are now discussed in detail.

Ultrafast Change of Oscillator Strength. The striking difference between the time-zero spectrum in water and DMSO was addressed in Figure 5.[60] It is evident in the UV ESA and SE bands. At time zero, they show smaller amplitude in water than in DMSO. The timescale on which the spectral difference arises is slower than optical (~1 fs, because absorption spectra in both solvents are apparently the same in the $S_1 \leftarrow S_0$ band) but ultrafast (not resolved): sequential contributions extracted from the global analysis show that the intensity of the SE peak is smaller in water than in DMSO even at time zero.[60] The difference is then established on a timescale faster than the time resolution ≤20 fs, which is compatible with ~500 cm^{-1} absorption spectral broadening, Figure 1. This apparent change of oscillator strength is also observed with 490 and 400 nm excitation.[60] It may be argued alternatively that the oscillator strength for SE and ESA does not change, but that an additional

TABLE 2: Fit Parameters for the Global Analysis of Transient Absorption Spectra of RF During the Earliest 2 ps (Upper Part) and Literature Values for Vibrational Frequencies (Lower Part)[a]

solvent	λ_{exc}/nm	τ_1/ps	τ_2/ps	ν_1/cm^{-1}	γ_1/ps^{-1}	ν_2/cm^{-1}	γ_2 /ps^{-1}	ν_3/cm^{-1}	γ_3/ps^{-1}
water	490	0.2	1.9						
water	440	0.2	1.1	91.7	4.2	196.8	6.1	286.9	2.1
water	400		0.7	77.8	5.3	174.9	2.7	283.6	0.9
DMSO[b]	490		1.2			170.2	7.3		
DMSO[c]	440		0.9	95.0	1.7	173.5	5.3	282.0	0.8
DMSO[c]	400		0.8	100.7	2.6	178.4	6.4	282.0	0.9
lumiflavin / ACN[d]	440		0.6	58.4	4.5	174.1	1.0		
Low Frequency Vibrational Modes From IR Spectroscopy									
τ(ribityl)[e]				50.7, 64.3, 99.5					
χ(isoalloxazine)[e]				73.7					
χ(pyrimidine)[e]				90.8					
χ(pyrimidine)[e]				125.2					
δ(isoalloxazine) in lumiflavin[e]						175.4			
δ(N_{10}-Me), δ(C_8-Me), δ(C_7-Me) in FMN[e,f]								300 and 261	

[a] Empty cells mean that the corresponding parameter was not used in the model. For instance, for 490 nm excitation in water (first row), a biexponential function was used, whereas for 440 nm in water, a biexponential function plus three oscillations were necessary. A minimum number of oscillations was used to model the experiment to noise level. They are understood as dominant modes, and they may slightly change with excitation wavelength and solvent. [b] Solvent oscillations were also fitted with ν_{1S} = 347.1 cm^{-1}, γ_{1S} = 1.8 ps^{-1} and ν_{2S} = 664.0 cm^{-1}, γ_{2S} = 0.9 ps^{-1}. [c] A low-frequency mode with ν_4 = 56.5, 52.4 cm^{-1} and γ_4 = 4.9, 3.1 ps^{-1} (λ_{exc} = 400, 440 nm, respectively) was also found. [d] Solvent oscillations show up with ν_{1S} = 380.3 cm^{-1}, γ_{1S} = 1.9 ps^{-1}. [e] Taken from Takahashi, M.; Ishikawa, Y.; Nishizawa, J. I.; Ito, H. *Chem. Phys. Lett.* **2005**, 475. τ stands for torsion, χ stands for for out-of-plane ring deformation, and δ stands for for in-plane ring deformation. [f] Taken from Copeland, R. A.; Spiro, T. G. *J. Phys. Chem.* **1985**, *90*, 6648.

state X* with ESA bands around 350 and 575 nm is excited only in water at time zero and decays independently. The latter option is unlikely. First, the stationary absorption spectra in water and DMSO are so alike (apart from a solvatochromic shift of the second optically-allowed transition, Figure 1) that a significant contribution of any transition other than $S_1 \leftarrow S_0$ can be safely ruled out for water solution. Second, if a new state X* were excited at time zero only in water, it is expected to deactivate differently. In contrast, the time evolution in both solvents is very much the same, Figures 2, 4 and 5, 6, despite the different weights of the SE and UV ESA bands, Figure 5. To reconcile these two observations (quasi-equal stationary absorption spectrum in water and DMSO but different early transient spectra), we propose a superposition state between the initially-excited S_1 and the X* state. The superposition is established on an ultrafast timescale in both solvents. The X*/S_1 population ratio depends on solvent, and a different degree of mixing explains the difference of oscillator strength between water and DMSO at early time. The process occurs in any solvent at comparable rate and hence induces similar absorption broadening (~500 cm^{-1}, Figure 1) whereas the extent of mixing depends on the specific interaction with the environment.

We discuss next the probable nature of the states involved and the coupling mechanism. $^1n\pi^*$ states lying close to the optically active S_1 ($^1\pi\pi^*$) are candidates for (i) weak absorption features on the blue edge of the $S_1 \leftarrow S_0$ transition and (ii) for the X* state being involved in the ultrafast process. Quantum mechanical calculations place the $^1n\pi^*$ states ~2000 cm^{-1} above the S_1 origin.[20,22,23] Direct excitation of the $^1n\pi^*$ states cannot explain additional absorption bands in the transient spectrum because the oscillator strength of the $^1n\pi^* \leftarrow S_0$ transitions is about 200 times smaller than that of $S_1 \leftarrow S_0$. Two scenarios can be proposed: the adiabatic and non-adiabatic coupling limits. Assume first that the $^1n\pi^*$ and $^1\pi\pi^*$ states couple adiabatically. In this case, the $^1n\pi^*$-rich state should show up in the optical spectrum as a weak shoulder on the blue flank of the parent $S_1 \leftarrow S_0$ transition. The coupling removes oscillator strength from the zero-order bright $S_1 \leftarrow S_0$ transition and places it into the zero-order dark $^1n\pi^* \leftarrow S_0$, but the oscillator strength is conserved

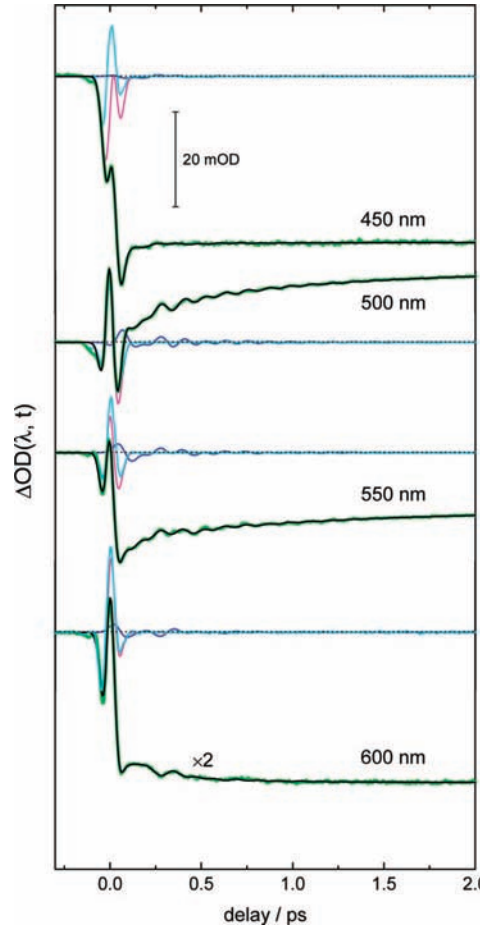

Figure 7. Global fit (thin black lines) of representative femtosecond transient absorption kinetic traces of riboflavin in water upon 440 nm excitation with parallel pump−probe polarization. Experimental kinetic traces are shown in thick green for the indicated probe wavelengths. Blue and magenta lines correspond to the oscillatory and coherent contributions, respectively, and the cyan line shows the non-resonant solvent signal. Black dotted lines mark the zero signal level for every probe wavelength.

when integrated over the main absorption band and the shoulder in the blue. The absorption broadening in Figure 1 may be then understood as an additional transition to the $^1n\pi^*$-rich state rather than lifetime broadening. Fluorescence is narrower and less probable than absorption because it occurs mainly from the $^1\pi\pi^*$-rich state, which is lower in energy. The second scenario is non-adiabatic coupling. If only S_1 ($\pi\pi^*$) is excited at time zero, strong coupling between the $^1\pi\pi^*$ and $^1n\pi^*$ states gives rise to oscillatory population transfer from $^1\pi\pi^*$ to $^1n\pi^*$ states which equilibrate at later delays.[65,66] When the coupling is strong (~100 cm^{-1}) and dephasing fast (10−20 fs), a superposition of the two coupled states may be formed on a 10 fs time scale.[65,66] The $S_1 \leftarrow S_0$ absorption band broadens now because of the short lifetime. Which extreme case applies depends on the time resolution compared to coupling strength, but both representations are indistinguishable in the strong coupling limit. There is however indication for the non-adiabatic limit: transient spectral differences between water and DMSO occur on a 20 fs timescale. They already demand 500 cm^{-1} absorption broadening. This observation leaves little room for blue-shifted absorption of the $^1n\pi^*$-rich state.

In summary, we propose that a mixture of $^1\pi\pi^* - {}^1n\pi^*$ states is attained by vibronic coupling along high-frequency modes. It occurs on a ~20 fs timescale after optical excitation. The degree of mixing depends on the environment, whereas the kinetics is essentially the same. This leads to equivalent absorption broadening in both solvents but to different mixing ratios in the excited state. The latter depend mainly on specific solute−solvent interactions.

Sub-Picosecond Exponential Contribution. Because isosbestic points are not observed, changes at early time appear to involve spectral diffusion. Decay times of 0.2 and 1.1 ps were fitted, and the spectral amplitudes are shown in Figure 8, top panel. They are negative at 500 nm and positive for $\lambda \geq 560$ nm, show vibronic structure with ~1300 cm^{-1} frequency, and are spectrally shifted against each other by ~700 cm^{-1}. This is consistent with the band integral analysis of Figure 4. Because of partial spectral overlap of ESA and SE, the process may be interpreted either as a rise of ESA around 500 nm or as decay of blue-shifted SE at early time. The dilemma may be solved by fluorescence up-conversion spectroscopy, where fluorescence dynamics is measured independently of ESA.[40] Up-conversion measurements show that most of the 240 cm^{-1} fluorescence shift occurs in the sub-picosecond timescale. The disagreement between the characteristic time constants from both experiments (0.2 and 1.1 ps versus 3.5 ps) is explained by the different apparatus functions of the pump−probe ($\tau_{cc} < 70$ fs) and fluorescence up-conversion setups ($\tau_{cc} = 2.6-3.5$ ps).[40] At higher time resolution, our pump−probe experiment shows evolution in the SE region during the earliest 2 ps only; the position of the SE band remains constant at later delays. Therefore, the fluorescence red shift in the up-conversion experiment follows the cross-correlation; that is, the response function is much faster than 3.5 ps. Sub-picosecond spectral relaxation in pump−probe spectroscopy monitors and resolves an apparent fluorescence red shift: decay of SE around 500 nm (negative amplitude of the exponential terms) and rise around 580 nm (positive amplitude).

The fluorescence shift exceeds substantially the 240 cm^{-1} of the up-conversion experiment[40] and follows solvation dynamics. It was shown by stationary spectroscopy that the Stokes shift in water (~4300 cm^{-1}) is ~900 cm^{-1} larger than that in the protein pocket. The difference may be attributed to the solvation contribution if equal intramolecular reorganization energies are assumed in both environments, which is reasonable. When experimental uncertainties are considered, the solvation contribution in water is substantially larger than the 240 cm^{-1} shift resolved by fluorescence up-conversion and expected to range between 500 and 1000 cm^{-1}. The estimate is consistent with our analysis of transient and stationary data, which indicates that fluorescence decays around 19500 cm^{-1}, Figure 8 top, and shifts to 18300 cm^{-1} at very late time, Figure 1.

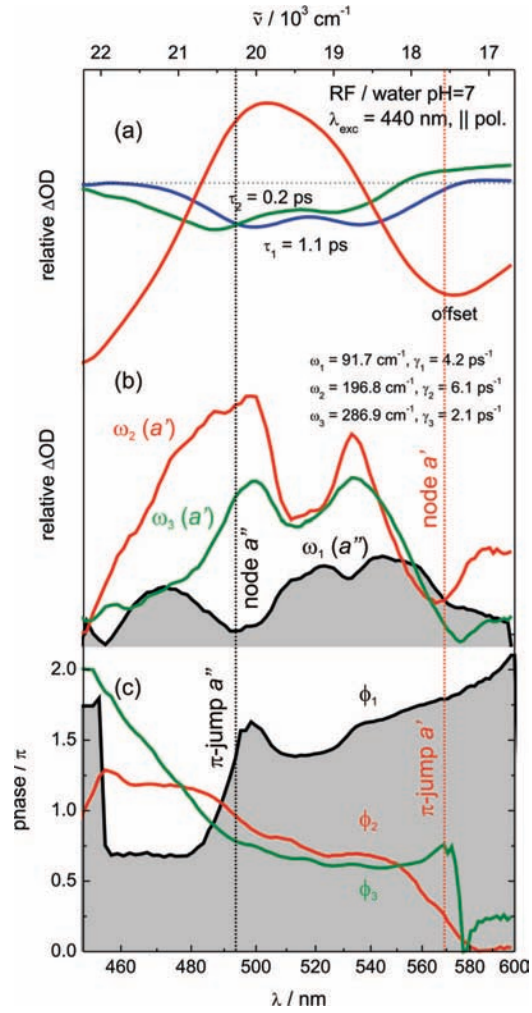

Figure 8. Global fit of femtosecond transient absorption spectra of riboflavin in water after excitation at 440 nm. Spectra were modelled as a sum of two exponentials plus three damped cosine-like oscillations. (a) Amplitudes associated with the exponential terms. Time constants are given as insets. (b) Amplitudes of oscillations, vertical dotted lines mark the positions of approximate nodes in the oscillation amplitude for a' (red) and a'' modes (black). The oscillation frequencies (ω_i) and their dephasing times (γ_i) are indictaed. (c) Time-zero phases (ϕ_i) of the cosine oscillations. Vertical dotted lines indicate the approximate π phase jump for out-of-plane (a'', black) and in-plane (a', red) modes.

The characteristic time constant of the process and how it is related to solvation dynamics is discussed next. Water dipolar solvation dynamics was studied by us with the model compound *N*-methyl-6-quinolone.[53] The solvation correlation function obtained from the normalized peak-shift function of SE, $S_\nu(t)$, shows biexponential behavior with time constants of 40 fs (40%) and 730 fs (60%). The resulting characteristic time constant for solvation is 0.5 ps. In turn, the femtosecond transient absorption dynamics of RF was modeled with a double-exponential function in the global analysis. Strong SE-ESA spectral overlap prevents resolving the SE band at early time and thereby

constructing the $S_\nu(t)$ function of SE. The time constants for RF are so-called decay-associated, as in the fluorescence up-conversion,[40] and cannot be compared directly to the decay components of the solvation correlation function. Instead, it is acceptable to estimate the characteristic time constant from the band integral in the region between 450 and 550 nm, which monitors the apparent rise of ESA. This yields a time constant $\langle\tau\rangle$ of 0.6 ± 0.1 ps in water, Figure 4, which matches the dipolar solvation time. $\langle\tau\rangle$ is independent of excitation wavelength as expected for solvation dynamics.

The change of dipole moment of RF upon excitation is estimated by dielectric continuum theory if a solvation shift of 500−1000 cm^{-1} is assumed. With a non-polarizable cavity of radius $a \approx 4-5$ Å, a S_0-S_1 dipole moment change $\Delta\mu$ of 2−3 Debye is obtained for a solvation shift ΔS of 240 cm^{-1}, eq 3. The dipole moment difference $\Delta\mu$ increases to at least 3−4 Debye if our 500 cm^{-1} lower limit for the solvation shift is taken and up to 4−6 Debye for the 1000 cm^{-1} higher limit. In other words, if only solvation dynamics is considered, continuum theory predicts a dipole moment change between 3 and 6 Debye.

$$\Delta\mu(\text{Debye}) = \sqrt{\frac{\Delta S h c a^3}{2\Delta f(\varepsilon, n)}}10^{18} \qquad (3)$$

How much does the continuum estimate approach to the true change of dipole moment remains an open question. Stationary absorption spectra show no solvatochromism, suggesting that the vertical $S_1 \leftarrow S_0$ transition bears no charge-transfer character.[19] The observation is in line with quantum mechanical calculations by Neiss et al., which predict no change of dipole moment upon $S_1 \leftarrow S_0$ excitation.[20] However, the characteristic times suggest that early processes are controlled by solvation. The latter implies a photoinduced change of dipole moment which provides the necessary driving force. We conjecture that the change in dipole moment is associated to $\pi\pi^*/n\pi^*$ mixing. Dipole moments of 5.4 and 1.9 D were calculated for the $n\pi^*$ states, [23] whereas the S_1 state shows much higher values, ∼10 D. [20,23] The small solvation contribution (∼10% of the Stokes shift) and the interplay between solvation dynamics and $\pi\pi^*/n\pi^*$ mixing prevents a more quantitative analysis at this stage.

Oscillatory Contribution. This contribution is characteristically weak for RF in polar solution. Only two or three modes could be identified unambiguously, Table 2. For instance, rapidly dephasing wavepackets with dominant frequencies of 92, 197, and 287 cm^{-1} were found upon excitation at 440 nm, Table 2 and Figure 8 bottom. The time-zero phases vary significantly with the probe wavelength.[60] This is taken as indication for vibrational wavepacket motion in contrast to coherent oscillations from vibronic coupling.[65,66] Because oscillations show significant amplitude both on the red edge of the bleach and on the SE band, Fig. 8 bottom, they map out coherent vibrational motion in the excited state.[67]

Four dominant oscillations are identified when comparing measurements in DMSO and water at different excitations. They show frequencies varying in the ranges 50−60, 70−100, and 170−200 and at 285 cm^{-1}, Table 2. These frequencies are obtained from a minimum set of damped non-chirped oscillations needed to describe the experiment to noise level in the bleach and SE regions. Fine details such as differences between ground- and excited-state frequencies, frequency chirp, or multimode contributions in a narrow frequency range (<50 cm^{-1}) are not resolvable in the time domain with our experimental conditions; we use the term dominant oscillation for that reason. Modes can be assigned crudely with the help of literature values for the ground electronic state of the flavin. The low-frequency vibrational spectrum of RF in the ground state was studied by Takahashi et al. up to 200 cm^{-1} by Terahertz spectroscopy.[68] The 175 cm^{-1} mode describes an in-plane deformation of the isoalloxazine. The dephasing constant of this mode is much smaller for lumiflavin (Scheme 1) in acetonitrile compared to RF in water or DMSO, which may indicate hydrogen-bonding interaction between the isoalloxazine moiety and its ribityl tail and with the solvent. At higher frequency, the 285 cm^{-1} oscillation is sharply defined and may correspond to the resonance Raman[69] peaks at 300 and 261 cm^{-1}. These modes are the in-plane bending of the $N_{10}-CH_2-$, C_7-Me, and C_8-Me bonds in flavin mononucleotide (FMN). Thus, in-plane deformation of the ring system is expected upon excitation to the S_1 state. We turn now to the low frequency modes in the 50−100 cm^{-1} range. They characterize out-of-plane bending motion of the aromatic moiety.[68] The torsion of the ribityl chain falls also in this spectral region but can be excluded because lumiflavin (lacking the ribityl chain) also shows sizeable sub-100 cm^{-1} activity, meaning that the amplitudes of all three modes are alike, Figure 8. Therefore, optical activity along out-of-plane modes (a'') is observed upon $S_1(A') \leftarrow S_0(A')$ transition of RF. The effect is quite remarkable because only totally symmetric modes are active in pure $A' \leftarrow A'$ electronic transitions.[70] $^1n\pi^* \leftrightarrow S_0$ transitions bear however oscillator strengths of about 100−200 times smaller than their $^1\pi\pi^* \leftrightarrow S_0$ counterparts in RF,[20,22,23] implying that excitation to the $^1n\pi^*$ states alone does not explain strong activity along a'' modes. This experimental finding demands $^1n\pi^* - ^1\pi\pi^*$ vibronic coupling which is then favoured by polar interactions and by excitation of low-frequency modes at room temperature.

A key piece of information is obtained from the spectral distribution of amplitudes and phases of oscillatory components, Figure 8b,c, respectively. For the out-of-plane mode with 92 cm^{-1} frequency, the amplitude shows a double-lobe structure with a node around 495 nm. The node occurs around the maximum of the exponential components as indicated by the black vertical dotted line. Exactly at this position, the phase changes steeply by a value between (3/4) π and π, as indicated in panel c. This resembles the way in which a vibrational wavepacket tunes the lineshape $L(\nu-\nu_0)$ of an electronic transition: the time-zero amplitude is approximately proportional to the first derivative of the lineshape squared $|(\partial L(\nu-\nu_0)/\partial\nu)|^2$ while the phase undergoes a π-jump around the band maximum ν_0.[65] High-frequency totally symmetric modes at 197 and 287 cm^{-1} behave similarly but exhibit a node around 570 nm, as indicated by the red dotted line. It is concluded that a'' and a' modes are localized in adjacent spectral regions. The very same behaviour is observed for all excitation wavelengths in water and DMSO.[60] Out-of-plane non-symmetric modes are thus active in the blue-shifted SE band, whereas in-plane totally symmetric modes are predominantly active in the red-shifted SE band. Therefore, blue SE is assigned to a $A'' \rightarrow S_0$ transition (predominantly $^1n\pi^* \rightarrow S_0$), whereas red SE has $A' \rightarrow S_0$ ($^1\pi\pi^* \rightarrow S_0$) character. Consistent with this interpretation is the fast dephasing time of the out-of plane mode: 0.2 ps, significantly faster than the solvation time of 0.5 ps in water. In contrast, the 287 cm^{-1} mode dephases with 0.5 ps.

In summary, solvation dynamics and intramolecular relaxation along low-frequency modes is proposed to occur during the earliest 2 ps. If only polar solvation is assumed for this time scale, a dipole moment change between 3 and 6 Debye is estimated from dielectric continuum theory. The estimate contrasts with high-level quantum mechanical calculations which predict no change of dipole moment upon $S_1 \leftarrow S_0$ excitation.[20,71]

SCHEME 2: Proposed Mechanism for the Ultrafast Excited-State Dynamics of Riboflavin in Polar Solution

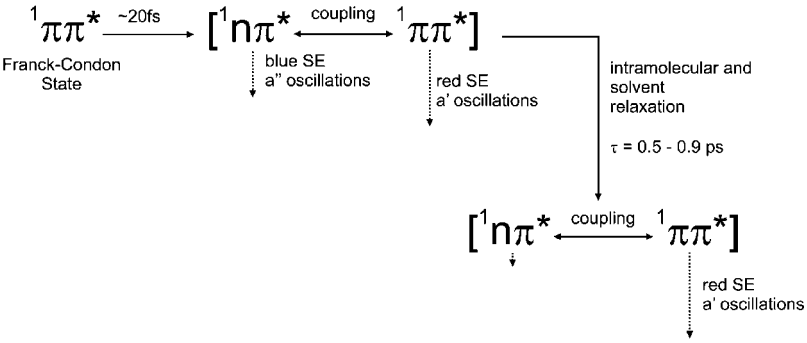

It is remarkable that, first, out-of-plane modes are optically active and, second, in-plane and out-of-plane modes emerge in different SE regions. This demonstrates coupling between the bright $^1\pi\pi^*$ state and closely lying A″ ($^1n\pi^*$) states. Coupling is enhanced by polar interactions and/or excitation of low-frequency modes at room temperature and becomes apparent just after optical excitation.[70] The population ratio between the coupled states is influenced by solvent dynamics.

Picosecond Dynamics. We turn now to the 100−400 ps time constants measured in water and DMSO.[60] These components show very small amplitude and are therefore determined with sizeable relative error, so that only qualitative explanations may be given. The picosecond time constant may correspond to the 36 ps component with negative amplitude observed in water by fluorescence up-conversion.[40] This time constant is much slower than solvation and has to be assigned to a distinct intramolecular process. It is interesting that the picosecond component is stronger upon excitation at 440 nm and shows very small amplitude upon red- and blue-edge excitations. This fact was already used in the results section to rule out vibrational cooling in the S_1 state as possible explanation. Furthermore, the spectral distribution of the picosecond time constant is such that the bleach appears to decay together with an ESA band in the UV, whereas the fluorescence becomes slightly more intense,[40] Figure 2d. In other words, evolution in the bleach region suggests that excited molecules return to the ground state. However, this is not compatible with a rise in fluorescence signal if only population dynamics is considered. To explain this apparent contradiction we propose that the cross-section for SE increases within 100−400 ps and that the decay in the bleach is due to an increase of ESA around 450 nm. Population does not return back to the ground state, but instead, an increase in the cross-section for SE and ESA occurs.

Conclusions

Femtosecond dynamics of riboflavin in polar solution was studied by broadband transient absorption spectroscopy. Three excitation wavelengths tuned to different parts of the first absorption band were employed. The spectral evolution shows tiny changes which, however, demonstrate rich photophysics. The mechanism is shown in Scheme 2. Time-zero spectra point to an apparent loss of oscillator strength occurring within the time resolution. The effect is most obvious in the stimulated emission band and is interpreted as the signature of ultrafast (< 20 fs) $\pi\pi^*-n\pi^*$ vibronic coupling. State mixing induces absorption broadening and decrease of transition dipole for $S_1 \rightarrow S_0$ emission. Population dynamics ensues with characteristic time constants of 0.6 and 0.9 ps in water and DMSO, respectively. The time constants are independent of excitation wavelength and consistent with solvation dynamics of solvatochromic dyes,[53,54] which indicates solvent control. Intramolecular reorganization along in- and out-of-plane bending modes is inferred by analysis of the oscillatory contribution to transient absorption. Out-of-plane and in-plane modes show up in adjacent regions of the SE band. This is understood as proof of mixed emission from $^1n\pi^*$- and $^1\pi\pi^*$-rich states at early time and as suggestion that vibronic coupling occurs with transfer of vibrational coherence.[49] In support, progressions along out-of-plane low-frequency modes (below 164 cm^{-1}) are not observed in the fluorescence excitation spectra of Lumiflavin in helium droplets (0.3 K).[70] It implies that vibrational wavepackets along out-of-plane low-frequency modes cannot be excited directly but by transfer of vibrational coherence from in-plane modes. Dynamics along the solvent coordinate enhances the $^1\pi\pi^*$ character of the superposition state.

Acknowledgment. The authors acknowledge support from the Cluster of Excellence "Unifying Concepts in Catalysis" coordinated by the Technische Universität Berlin and funded by the Deutsche Forschungsgemeinschaft. We gratefully acknowledge the photochemistry group of the University of Santiago de Compostela (USC, Spain) for the fluorescence lifetime measurements. Manuel Mosquera (USC) and Sergey Kovalenko and Niko Ernsting (Humboldt University of Berlin, HUB) are also acknowledged for critical readings of the manuscript. Peter Hegemann (HUB) is acknowledged for support.

Supporting Information Available: Spectral evolution of RF in water and DMSO upon 490 and 400 nm excitation, global analysis of femtosecond transient absorption data of RF in water and DMSO for 400 and 490 nm excitations, estimated triplet−triplet transient absorption spectra and transient anisotropy. This material is available free of charge via the Internet at http://pubs.acs.org.

References and Notes

(1) van der Horst, M.; Hellingwerf, K. J. *Acc. Chem. Res.* **2004**, *37*, 13.

(2) Hellingwerf, K. J. *J. Photochem. Photobiol. B: Biol.* **2000**, *54*, 94.

(3) Losi, A. *Photochem. Photobiol.* **2007**, *83*, 1283.

(4) Gauden, M.; Yeremenko, S.; Laan, W.; van Stokkum, I. H. M.; Ihalainen, J. A.; van Grondelle, R.; Hellingwerf, K. J.; Kennis, J. T. M. *Biochem.* **2005**, *44*, 3653.

(5) Unno, M.; Sano, R.; Masuda, S.; Ono, T.; Yamauchi, S. *J. Phys. Chem. B* **2005**, *109*, 12620.

(6) Masuda, S.; Hasegawa, K.; Ishii, A.; Ono, T. *Biochem.* **2004**, *43*, 5304.

(7) Masuda, S.; Hasegawa, K.; Ono, T. *Biochem.* **2005**, *44*, 1215.

(8) Gauden, M.; van Stokkum, I. H. M.; Key, J. M.; Lührs, D. Ch.; van Grondelle, R.; Hegemann, P.; Kennis, J. T. M. *Proc. Natl. Acad. Sci. U. S. A.* **2006**, *103*, 10895.

(9) Salomon, M.; Christie, J. M.; Knieb, E.; Lempert, U.; Briggs, W. R. *Biochemistry* **2000**, *39*, 9401.
(10) Salomon, M.; Eisenreich, W.; Dürr, H.; Sleicher, E.; Knieb, E.; Massey, V.; Rüdiger, W.; Müller, F.; Bacher, A.; Richter, G. *Proc. Natl. Acad. Sci. U. S. A.* **2001**, *98*, 12357.
(11) Crosson, S.; Moffat, K. *Plant Cell* **2002**, *14*, 1067.
(12) Fedorov, R.; Schlichting, I.; Hartmann, E.; Domratcheva, T.; Fuhrmann, M.; Hegemann, P. *Biophys. J.* **2003**, *84*, 2474.
(13) Kottke, T.; Batschauer, A.; Ahmad, M.; Heberle, J. *Biochemistry* **2006**, *45*, 2472.
(14) Dudley, K. H.; Ehrenberg, A.; Hemmerich, P.; Müller, F. *Helv. Chim. Act.* **1964**, *47*, 1354.
(15) Drössler, P.; Holzer, W.; Penzkofer, A.; Hegemann, P. *Chem. Phys.* **2002**, *282*, 429.
(16) Visser, A. J. W. G.; Müller, F. *Helv. Chim. Acta* **1979**, *62*, 593.
(17) Harbury, H. A.; LaNoue, K. F.; Loach, P. A.; Amick, R. M. *Proc. Natl. Acad. Sci. U. S. A.* **1959**, *45*, 1708.
(18) Kotaki, A.; Naoi, M.; Okuda, J.; Yagi, K. *J. Biochem.* **1967**, *61*, 404.
(19) Stanley, R. J.; Jang, H. *J. Phys. Chem. A* **1999**, *103*, 8976.
(20) Neiss, C.; Saalfrank, P.; Parac, M.; Grimme, S. *J. Phys. Chem. A* **2003**, *107*, 140.
(21) Insinska-Rak, M.; Sikorska, E.; Herance, J. R.; Bourdelande, J. L.; Khmelinskii, I. V.; Kubicki, M.; Prukala, W.; Machado, I. F.; Komasa, A.; Ferreira, L. F. V.; Sikorski, M. *Photochem. Photobiol. Sci.* **2005**, *4*, 463.
(22) Sikorska, E.; Khmelinskii, I.; Komasa, A.; Koput, J.; Ferreira, L. F. V.; Herance, J. R.; Boudelande, J. L.; Williams, S. L.; Worrall, D. R.; Insinska-Rak, M.; Sikorski, M. *Chem. Phys.* **2005**, *314*, 239.
(23) Climent, T.; González-Luque, R.; Merchán, M.; Serrano-Andrés, L. *J. Phys. Chem. A* **2006**, *110*, 13584.
(24) Domratcheva, T.; Fedorov, R.; Schlichting, I. *J. Chem. Theory Comput.* **2006**, *2*, 1565.
(25) Weber, G.; Teale, F. W. J. *Trans. Faraday Soc.* **1957**, *53*, 646.
(26) Weber, G. *Biochem. J.* **1950**, *47*, 114.
(27) Porcal, G.; Bertolotti, S. G.; Previtali, C. M.; Encinas, M. V. *Phys. Chem. Chem. Phys.* **2003**, *5*, 4123.
(28) Penzkofer, A.; Bansal, A. K.; Song, S. H.; Dick, B. *Chem. Phys.* **2007**, *336*, 14.
(29) Penzer, G. R.; Radda, G. K. *Biochem. J.* **1968**, *109*, 259.
(30) Drössler, P.; Holzer, W.; Penzkofer, A.; Hegemann, P. *Chem. Phys.* **2003**, *286*, 409.
(31) Mataga, N.; Chosrowjan, H.; Shibata, Y.; Tanaka, F. *J. Phys. Chem. B* **1998**, *102*, 7081.
(32) Mataga, N.; Chosrowjan, H.; Shibata, Y.; Tanaka, F.; Nishina, Y.; Shiga, K. *J. Phys. Chem. B* **2000**, *104*, 10667.
(33) Mataga, N.; Chosrowjan, H.; Taniguchi, S.; Tanaka, F.; Kido, N.; Kitamura, M. *J. Phys. Chem. B* **2002**, *106*, 8917.
(34) Chosrowjan, H.; Taniguchi, S.; Mataga, N.; Tanaka, F.; Visser, A. J. W. G. *Chem. Phys. Lett.* **2003**, *378*, 354.
(35) Stanley, R. J.; MacFarlane, A. W., IV *J. Chem. Phys. A* **2000**, *104*, 6899.
(36) Islam, S. D. M.; Penzkofer, A.; Hegemann, P. *Chem. Phys.* **2003**, *291*, 97.
(37) Heelis, P. F. *Chem. Soc. Rev.* **1982**, *11*, 15.
(38) Song, P. S. *Int. J. Quan. Chem* **1969**, *3*, 303.
(39) Sun, M.; Moore, T. A.; Song, P. S. *J. Am. Chem. Soc.* **1972**, *94*, 1730.
(40) Petushkov, V. N.; van Stokkum, I. H. M.; Gobets, B.; van Mourik, F.; Lee, J.; van Grondelle, R.; Visser, A. J. W. G. *J. Phys. Chem. B* **2003**, *107*, 10934.
(41) Kondo, M.; Nappa, J.; Ronayne, K. L.; Stelling, A. L.; Tonge, P. J.; Meech, S. R. *J. Phys. Chem. B* **2006**, *110*, 20107.
(42) Zhong, D.; Zewail, A. H. *Proc. Natl. Acad. Sci. U. S. A.* **2001**, *98*, 11867.
(43) Kennis, J. T. M.; Crosson, S.; Gauden, M.; van Stokkum, I. H. M.; Moffat, K.; van Grondelle, R. *Biochem.* **2003**, *42*, 3385.
(44) Kennis, J. T. M.; van Stokkum, I. H. M.; Crosson, S.; Gauden, M.; Moffat, K.; van Grondelle, R. *J. Am. Chem. Soc.* **2004**, *126*, 4512.
(45) Gauden, M.; Yeremenko, S.; Laan, W.; van Stokkum, I. H. M.; Ihalainen, J. A.; van Grondelle, R.; Hellingwerf, K. J.; Kennis, J. T. M. *Biochem.* **2005**, *44*, 3653.
(46) Lann, W.; Gauden, M.; Yeremenko, S.; van Grondelle, R.; Kennis, J. T. M.; Hellingwerf, K. J. *Biochem.* **2006**, *45*, 51.
(47) Gauden, M.; Grinstead, J. S.; Laan, W.; van Stokkum, I. H. M.; Avila-Perez, M.; Toh, K. C.; Boelens, R.; Kaptein, R.; van Grondelle, R.; Hellingwerf, K. J.; Kennis, J. T. M. *Biochem.* **2007**, *46*, 7405.
(48) Kovalenko, S. A.; Dobryakov, A. L.; Ruthmann, J.; Ernsting, N. P. *Phys. Rev. A* **1999**, *59*, 2369.
(49) Jean, J. M. *J. Chem. Phys.* **1994**, *101*, 10464.
(50) Birks, J. B. *Photophysics of aromatic molecules*; Wiley-Interscience: New York, 1970; Sections 3 and 4.
(51) Melhuish, W. *J. Phys. Chem.* **1961**, *65*, 229.
(52) Karstens, T.; Kobs, K. *J. Phys. Chem.* **1980**, *84*, 1871.
(53) Lustres, J. L. P.; Kovalenko, S. A.; Mosquera, M.; Senyushkina, T.; Flasche, W.; Ernsting, N. P. *Angew. Chem. Int. Ed.* **2005**, *44*, 2.
(54) Horng, M. L.; Gardecki, J. A.; Papazyan, A.; Maroncelli, M. *J. Phys. Chem.* **1995**, *99*, 17311.
(55) Mühlpfordt, A.; Schanz, R.; Ernsting, N. P.; Fartzdinov, V.; Grimme, S. *Phys. Chem. Chem. Phys.* **1999**, *1*, 3209.
(56) Strickler, S. J.; Berg, R. A. *J. Chem. Phys.* **1962**, *37*, 814.
(57) Fee, R. S.; Maroncelli, M. *Chem. Phys.* **1994**, *183*, 235.
(58) Holzer, W.; Penzkofer, A.; Hegemann, P. *Chem. Phys.* **2005**, *308*, 79.
(59) Lewis, J. E.; Maroncelli, M. *Chem. Phys. Lett.* **1998**, *282*, 197.
(60) See Supporting information.
(61) Schwarzer, D.; Troe, J.; Zerezke, M. *J. Chem. Phys.* **1997**, *107*, 8380.
(62) The solvation correlation function of water was empirically fitted to a biexponential function with time constants 0.04 ps (40%) and 0.73 ps (60%). Alternatively, the function may be also fitted to a Gaussian (ω = 0.03 ps, 26%) plus two exponentials: 0.15 ps (11%) and 0.75 (63%).[53] To compare with the τ_{1e} times published by Horng et al. for an extensive series of solvents,[54] the solvation correlation function was fitted monoexponentially resulting on a τ_{1e} of 0.5 ps.
(63) The system of linear equations can be written in matrix form as $\mathbf{A}(n_{delay}$ by $n_c)\mathbf{X}(n_c$ by $n_\lambda) = \mathbf{Y}(n_{delay}$ by $n_\lambda)$, where the quantities in parenthesis give the dimensions of the matrixes (boldface). n_{delay} is the number of pump−probe delays scanned, n_λ is the total number of probe wavelengths, and n_c is the number of kinetic components included in the analysis. **A** contains the traces of the kinetic components and depends on model parameters as pump−probe cross-correlation, rate constants, vibrational frequencies, and damping rates. The model parameters are optimized by a non-linear least squares routine to minimize the difference between the model **Y** and the experiment $\Delta OD(t,\lambda)$.
(64) Equation 2 only shows cos oscillations. Indeed, oscillations were fitted with $\sin(\omega t)$ and $\cos(\omega t)$ functions for each frequency with zero initial phase. The pure cosine oscillation was then reconstructed from the sum-angle trigonometric relationships, and the time-zero phase of the pure cosine function can then be obtained between 0 and 2π with avoidance of the intrinsic phase uncertainty resulting from the symmetry of the cosine function.
(65) Kovalenko, S. A.; Dobryakov, A. L.; Fartzdinov, V. *Phys. Rev. Lett.* **2006**, *96*, 068301.
(66) Lustres, J. L. P.; Dobryakov, A. L.; Holzwarth, A.; Veiga, M. *Angew. Chem. Int. Ed.* **2007**, *46*, 3758.
(67) Dobryakov, A. L.; Ersnting, N. P. *Chem. Phys.*. submitted.
(68) Takahashi, M.; Ishikawa, Y.; Nishizawa, J.; Ito, H. *Chem. Phys. Lett.* **2005**, *401*, 475.
(69) Copeland, R. A.; Spiro, T. G. *J. Phys. Chem.* **1986**, *90*, 6648.
(70) Alexander Vdovin, Alkwin Slenczka, Bernhard Dick, Institut für Physikalische und Theoretische Chemie, Universität Regensburg. The fluorescence excitation and emission spectra of lumiflavin in Helium nanodroplets (at 0.3 K) are void of signals below 164 cm^{-1}. This observation may indicate that out-of-plane modes are not optically active in the droplets at 0.3 K or else that these modes are strongly damped in the He first solvation shell. Private communication **2008**.
(71) Salzmann, S.; Tatchen, J.; Marian, C. M. *J. Photochem. Photobiol. A: Chem.* **2008**, *198*, 221. This recent paper confirms the dipole moments and oscillator strengths calculated by Neiss et al. (ref 20). Dipole moments (μ): 8.20 (S_0), 9.75 (S_1), 4.17 (S_2), and 3.95 Debye (S_3). Oscillatos strength: 0.2849 (S_1←S_0), 0.0025 (S_2←S_0), and 0.0007 (S_3←S_0).

JP805962U